Moist Hadley Circulation: Possible Role of Wave–Convection Coupling in Aquaplanet Experiments

TAKESHI HORINOUCHI

Faculty of Environmental Earth Science, Hokkaido University, Sapporo, Japan

(Manuscript received 25 May 2011, in final form 24 August 2011)

ABSTRACT

Aquaplanet simulations for a given sea surface temperature (SST) are conducted to elucidate possible roles of transient variability in the Hadley circulation and the intertropical convergence zone (ITCZ). Their roles are best illustrated with globally uniform SSTs. For such SSTs, an ITCZ and a Hadley circulation that are nearly equatorially symmetric emerge spontaneously. Their strength varies over a wide range from being faint to climatologically significant depending on a tunable parameter of the model's cumulus parameterization. In some cases asymmetric Hadley circulations formed along with long-lived tropical cyclones.

The tunable parameter affects the transient variability of tropical precipitation. In the runs in which well-defined near-symmetric ITCZs formed, tropical precipitation exhibited clear signatures of convectively coupled equatorial waves. The waves can explain the concentration of precipitation to the equatorial region, which induces the Hadley circulation. Also, the meridional structures of simulated ITCZs are consistent with the distribution of convergence/divergence associated with dominant equatorial wave modes.

Even when the pole–equator temperature gradient is introduced, the dependence of the strength of the circulation to transient disturbances remains. Therefore, transient variability may have a broader impact on tropical climate and its numerical modeling than has been thought.

The reason that a wide variety of circulation is possible when the SST gradient is weak is because the distribution of latent heating can be interactively adjusted while a circulation is formed. Angular momentum budget does not provide an effective thermodynamic constraint, since baroclinic instability redistributes the angular momentum.

1. Introduction

The Hadley circulation and the intertropical convergence zone (ITCZ) are important components of the general circulation of the earth's atmosphere. A historically important and influential theory of the Hadley circulation is proposed by Held and Hou (1980, hereafter HH). HH offered a theory of the axisymmetric circulation that is driven thermally by Newtonian relaxation toward a radiative equilibrium temperature, which has a $\cos^2\phi$ dependence on latitude ϕ. The HH model is able predict a number of features of the Hadley circulation such as the meridional extent and the strength (if the relaxation time scale is given). It can also be extended to equatorially asymmetric cases to show that a heating maximum centered off the equator effectively drives the circulation (Lindzen and Hou 1988).

Later studies have shown that extratropical eddies affect the Hadley circulation substantially (e.g., Schneider 1984; Satoh et al. 1995; Becker et al. 1997; Walker and Schneider 2006). Using an idealized aquaplanet global model, Satoh et al. (1995) demonstrated that the Hadley circulation is enhanced and widened by vertical angular momentum transport in baroclinic eddies. Walker and Schneider showed the scaling relations of the Hadley circulation depending on a number of external parameters such as the planet radius, the rotation rate, and thermal conditions.

The distribution of the sea surface temperature (SST), which is given in aquaplanet simulations or in atmospheric general circulation models (AGCMs), is in reality affected by the atmospheric circulation. Thus, an understanding of the Hadley circulation and the ITCZ should eventually be placed in the context of a coupled atmosphere–ocean system (e.g., Xie and Philander 1994;

Corresponding author address: Takeshi Horinouchi, Faculty of Environmental Earth Science, Hokkaido University, N10W5 Sapporo, Hokkaido 060-0810, Japan.
E-mail: horinout@ees.hokudai.ac.jp

DOI: 10.1175/JAS-D-11-0149.1

Xie 2005). Understanding how the atmosphere responds to prescribed SST is a critical step toward this understanding, which is actually not straightforward as reviewed below.

The ITCZ tends to be situated along zonally oriented SST peaks off the equator. Lindzen and Nigam (1987) proposed a simple theory with which climatological convergence in the tropical boundary layer is driven by SST gradients. While a part of the convergence contributes to the shallow boundary layer circulation (Zhang et al. 2004), a large portion of the remaining contributes to deep upwelling associated with the ITCZ. The extent to which the Lindzen and Nigam theory is applicable has been argued substantially, but recently Back and Bretherton (2009) showed its validity using a skillful linear mixed layer model and observational (satellite and reanalysis) data.

In numerical atmospheric models, however, a variety exists among the simulated relationship between the tropical precipitation and SST (e.g., Biasutti et al. 2006). Early studies by Numaguti (1993) and Hess et al. (1993) showed that in aquaplanet general circulation models with SST peaking at the equator, both single and double ITCZs can form depending on the cumulus parameterization used (in their cases, the moist convective adjustment scheme for the single ITCZ and the Kuo scheme for the double ITCZ). Although most modern AGCMs do not use Kuo-type closures based on moisture convergence, many of them still suffer the ''double ITCZ syndrome'' to a varying extent, which sometimes occurs in combination with SST biases in coupled GCMs (Lin 2007; Bretherton 2007).

There have been theoretical studies that emphasized the role of dynamics in control of the location of the ITCZ (Charney 1971; Bellon and Sobel 2010, and references there in). In this context, Holton et al. (1971) proposed that the equatorial waves subject to the conditional instability of the second kind (CISK) may contribute to the off-equatorial location of the ITCZ. Hess et al. (1993) also suggested the role of zonally asymmetric equatorial disturbances in the control of the ITCZ by comparing three-dimensional and two-dimensional axisymmetric aquaplanet AGCM experiments. However, the possible roles of equatorial disturbances have not drawn much attention in most of the literature on the ITCZ and the Hadley circulation. Also, there is an observational study against it (Gu and Zhang 2002).

As will be shown in the rest of this paper, the role of the equatorial disturbances can be illustrated in a clear manner by using aquaplanet experiments with globally uniform SST. The AGCM studies with such an SST can be reviewed as follows. It has been shown that structures like the ITCZ and the Hadley circulation often emerge in aquaplanet experiments even with globally uniform SST (Sumi 1992; Horinouchi and Yoden 1998; Kirtman and Schneider 2000; Chao and Chen 2004; Barsugli et al. 2005). Kirtman and Schneider obtained a well-defined ITCZ centered on the equator using an aquaplanet experiment with globally uniform SST. They further conducted an experiment with a coupled oceanic mixed layer model under globally uniform solar insolation. In this case the SST predicted in the model was minimized at the equator, but the ITCZ, though weaker, was formed around the equator. Barsugli et al. extended the study of Kirtman and Schneider and found multiple forms of equilibria depending on the values of the globally uniform solar insolation: an equatorially symmetric double ITCZ, a near-symmetric single ITCZ, a transient asymmetric ITCZ, and a stable, strongly asymmetric ITCZ. Hysteresis and multiple equilibria were also found. In their study, asymmetric equilibria were not obtained with their atmosphere-only model with globally uniform SST. However, Chao and Chen (2004) obtained both symmetric and asymmetric ITCZs depending on model settings with prescribed globally uniform SST. Raymond (2000) used a two-dimensional (latitude vs altitude) model and showed that in the presence of the cloud–radiation feedback, an equatorially asymmetric Hadley circulation formed over uniform SST.

In this study, aquaplanet simulations are conducted to elucidate possible roles of transient equatorial disturbances in the control of the Hadley circulation and the ITCZ. A special focus is on the cases conducted using globally uniform SST, where a meridional circulation cannot form under the HH theory. It is shown that the strength of the ''Hadley circulation'' over the uniform SST varies from being faint to substantial (comparable that in the real atmosphere) depending on the activity of the convectively coupled equatorial waves. Here, their activity is controlled by a subcloud relative humidity threshold on the triggering of the cumulus parameterization (see section 2). The waves affect not only the strength of the circulation but also the fine structure of the simulated ITCZ. Experiments with latitudinally varying SST are shown to show the relevance of the findings to more realistic SST distributions with a pole–equator temperature gradient.

The aforementioned studies using the global uniform SST indicate that there is a substantial degree of freedom regarding the structure and the strengths of the ITCZ and the Hadley circulation for a given SST. However, these studies did not explicitly explain why a large variability is possible in terms of the thermodynamic constraints. The task is undertaken in this study.

The rest of the paper is organized as follows. The model and the numerical experiments are introduced in section 2. Results from the runs using globally uniform

TABLE 1. Summary of the numerical experiment series. Nonstandard settings and the value of ϕ_0 when $\Delta_S \neq 0$ are denoted in the "Others" field. Some runs (the $\Omega/\Omega_E = 1$ run in RotChg and the $\Delta_S = 0$ runs in Y2-eq and Y2–10N) are the same runs as in the Cntrl series.

Series name	T_0 (K)	Δ_S (K)	RH_C	Others
Cntrl	299	0	0, 0.3, 0.4, 0.5 0.6, 0.7, 0.8, 0.9	
4-Col	299	0	0, 0.3, 0.7, 0.9	Four-color radiation
AMSI	299	0	0, 0.3, 0.5, 0.7, 0.9	ϕ-dependent solar insolation
T0Chg	293, 302	0	0, 0.3, 0.5, 0.7, 0.9	
Eqdmp	299	0	0.7	Equatorial eddy damping
Axsym	299	0	0.7	Axisymmetric runs
RotChg	299	0	0.7	$\Omega/\Omega_E = 1, 1/2, 1/4$
Y2-eq	299	0, 5, 10, 20, 40	0, 0.3, 0.5, 0.7, 0.9	$\phi_0 = 0°$
Y2–10N	299	0, 5, 10, 20, 40	0, 0.7	$\phi_0 = 10°$N

SST are presented in section 3. The results are further examined in section 4 to elucidate possible roles of convectively coupled disturbances. Results using latitudinally dependent SST are investigated in section 5. Discussion is presented in section 6 of the thermodynamic constraints and the angular momentum budget. Conclusions are drawn in section 7.

2. Model and experiments

The model used is the University of Tokyo Center for Climate System Research–National Institute for Environmental Studies–Frontier Research Center for Global Chance (CCSR/NIES/FRCGC) AGCM version 5.6 (Hasumi and Emori 2004). Numerical experiments are made with the T42 horizontal resolution. The entire surface is assumed to be the ocean with prescribed SST. The number of vertical levels taken is 25, where 19 levels are below the 0.1-sigma level, and the greatest sigma level is 0.0027. Rayleigh friction is exerted in the stratosphere with the coefficient increasing with altitude up to 30^{-1} day^{-1}. Analysis is made after interpolating model outputs, which are daily mean values, onto the standard pressure levels.

The cumulus parameterization of the model is the prognostic Arakawa–Schubert scheme on which an additional constraint is introduced to limit the triggering of deep convection if the subcloud relative humidity is under a threshold value RH_C. The model's standard setting of RH_C is 0.8 (80%). The introduction of RH_C to this model improved a bias that the variability of tropical rainfall is too small (Emori et al. 2005). Note that a similar thresholding is introduced in many AGCMs (Gregory and Miller 1989; Sud and Walker 1999; Zhang and Mu 2005; Li et al. 2007). In this study RH_C is treated as an ad hoc controllable parameter, rather than an object of tuning, to modify the behavior of parameterized convection.

In most experiments, the model's standard radiation scheme (Nakajima et al. 2000) is used, but the solar insolation is assumed to be steady and globally uniform equal to the annual- and global-mean value. In a series, a simplified four-color radiation scheme is used. This scheme is not tuned much and is found to cause unrealistically excessive cooling by low-level clouds by as much as >10 K day^{-1}. Therefore, the results obtained with it should not be emphasized much. They are nonetheless shown in this paper since the results are of some interest from a dynamical point of view.

The vertical eddy diffusion is parameterized by the Mellor–Yamada level-2 scheme. The horizontal diffusion is of eighth order ($\propto\nabla^8$), and the e-folding time for the greatest total wavenumber of 42 is 1 day.

SSTs of all the series can be expressed as

$$\mathrm{SST} = T_0 + \Delta_s(\mu - \mu_0)^2, \tag{1}$$

where $\mu \equiv \sin\phi$, and Δ_S, T_0, and μ_0 ($=\sin\phi_0$) are constants. When SST maximizes on the equator ($\mu_0 = 0$), Δ_S is the pole-to-equator SST difference. In many series including the control series, named Cntrl, SST is set to 299 K uniformly over the globe ($T_0 = 299$ K and $\Delta_S = 0$).

The numerical experiments reported are outlined in Table 1. Nonstandard settings that have not been described are as follows. In the series AMSI (standing for the annual-mean solar insolation), solar insolation is set to the annual mean value for each latitude. In the series Eqdmp, the Rayleigh friction with an e-folding time of 2 days is exerted on the perturbation horizontal winds (defined as the deviation from the zonal mean) between 10°N and 10°S. In the series Axsym, the axisymmetric version of the model is used with the same meridional resolution. In the series RotChg, the angular frequency of the planetary rotation Ω is changed; in the other series, it is set to equal to the earth's value Ω_E.

The initial condition of all runs is a resting isothermal atmosphere of 299 K with a small large-scale temperature perturbation, and the model was run for 720 days (expressed as 2 yr hereafter) or 1440 days (4 yr). Although

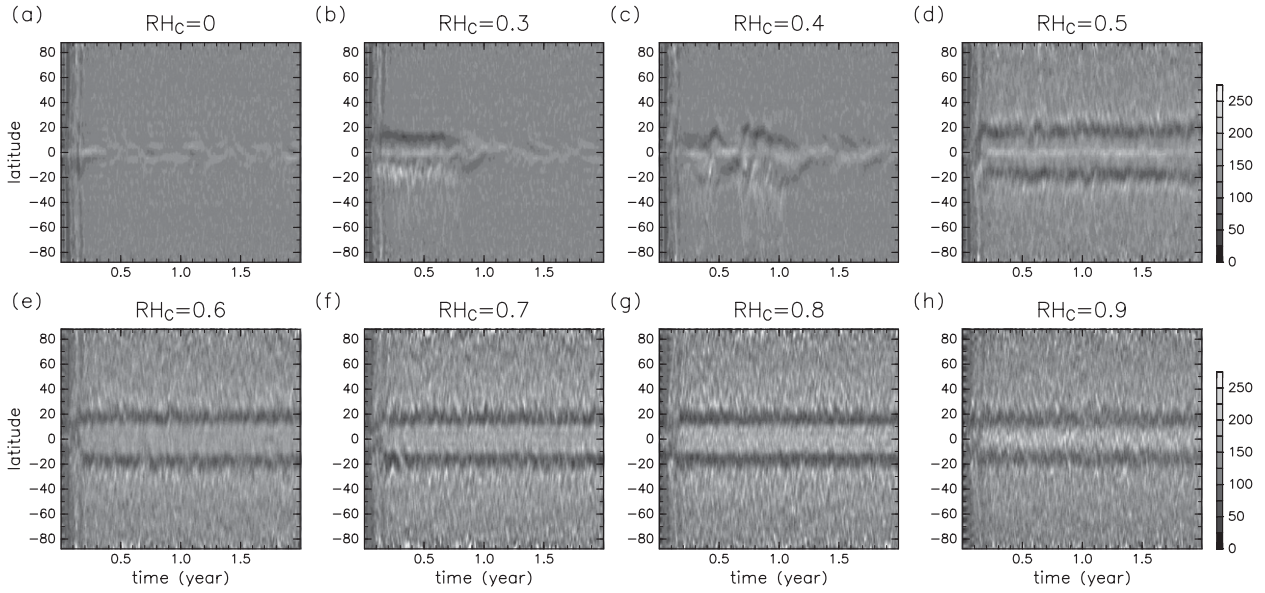

FIG. 1. Time–latitude sections of zonal mean precipitation (W m^{-2}; expressed in terms of latent heating) for the first 2 yr of the Cntrl runs. The RH_C values are shown above the panels.

the statistics presented in this paper are made for the second model year, checks were made for the third and fourth years in many cases, and the validity was confirmed.

3. Mean precipitation and circulation when SST is uniform

In the Cntrl series, SST is set uniformly to 299 K, and RH_C is varied. Figure 1 shows the time evolution of the zonal mean precipitation. For $RH_C \geq 0.5$, persistent latitudinal structures emerge spontaneously in the tropics in the first year and last until the end of the fourth year (not shown). Figure 2 shows precipitation averaged over the second model year. An enhancement in the equatorial region and suppression at higher latitudes in the tropics are found when $RH_C \geq 0.5$, although SST is globally uniform. The equatorial enhancement is referred to as the ''ITCZ'' in what follows. Precipitation is nearly

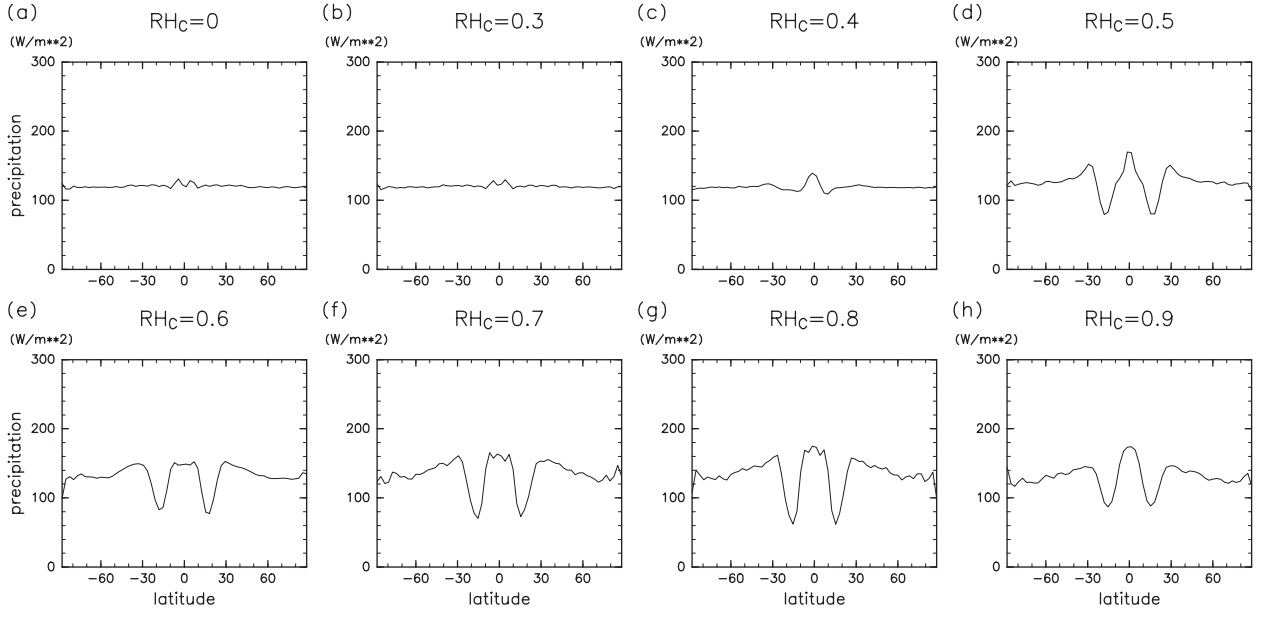

FIG. 2. Meridional distribution of zonal mean precipitation (W m^{-2}) averaged over the second model year of the Cntrl runs.

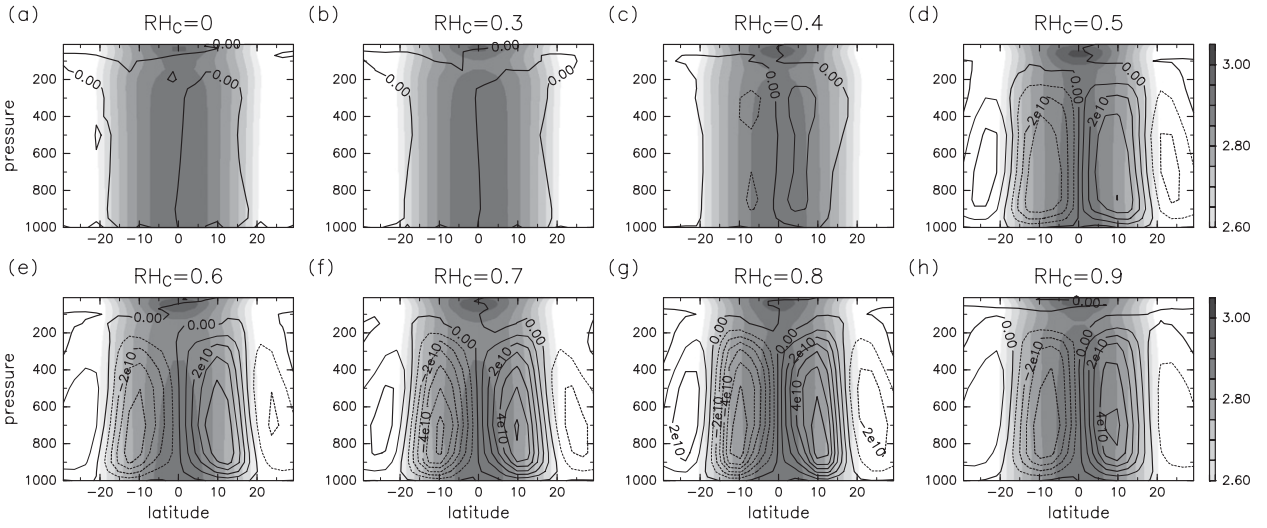

FIG. 3. Meridional mass streamfunction Ψ (contours; contour interval = 2×10^{10} kg s^{-1}) and the absolute angular momentum $\overline{m}$ (shading; interval = 0.05×10^{9} m^2 s^{-1}) averaged over the second model year of the Cntrl runs.

globally uniform for $RH_C \leq 0.3$, and a small equatorial maximum is found when $RH_C = 0.4$.

Figure 3 shows the meridional mass streamfunction Ψ derived numerically based on

$$\overline{v} = \frac{g\,\partial\Psi}{2\pi R_E \cos\phi \partial p}, \tag{2}$$

where $\overline{v}$ is the zonal mean meridional wind, g is gravity, R_E is the earth's radius, and p is pressure. Corresponding to the precipitation distribution shown in Fig. 2, circulations like the Hadley circulation (hereafter simply called the Hadley circulation, or Hadley cells) form. Its strength at large RH_C is substantial, being comparable to or greater than the half of the observed climatological mass flux in the equinoctial seasons. The width of each of the Hadley cells is about 20° irrespective of the values of RH_C, which is smaller than that in the real atmosphere. Figure 3 also shows the absolute angular momentum

$$\overline{m} \equiv R_E \cos\phi(\Omega R_E \cos\phi + \overline{u}), \tag{3}$$

which is investigated in section 6b (here $\overline{u}$ is the zonal-mean zonal wind).

These results are similar in the AMSI series in which latitudinally dependent annual-mean solar insolation is used (not shown). In the AMSI runs, the meridional distribution of mean precipitation has a slightly different ϕ dependence in the extratropics, but the precipitation and the circulation in the tropics are similar to those in the Cntrl runs.

Figure 4 shows the upward mass flux associated with the Hadley circulation in the Cntrl runs (filled squares). The strength of the Hadley circulation is increased as the value of RH_C is increased from 0 to 0.8 by more than 10 times and it is slightly decreased when RH_C is further increased to 0.9. It is noteworthy that altering a tunable parameter of cumulus parameterization (here, RH_C) can vary the meridional circulation to a large extent in

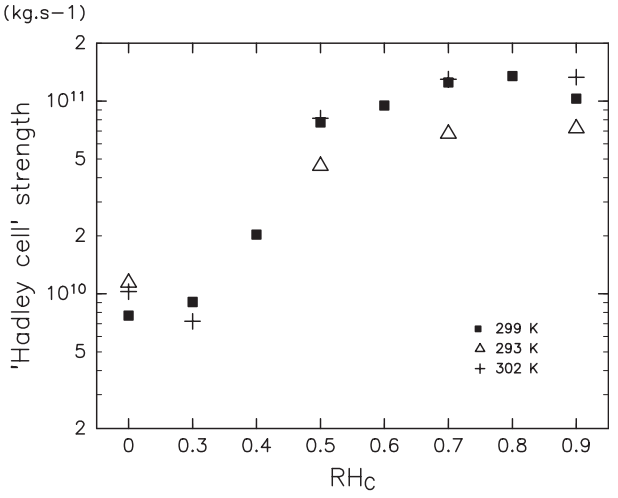

FIG. 4. Upward mass flux associated with the Hadley circulation $\Delta\Psi_{600}$ (see below) in the Cntrl runs (T_0 = 299 K, filled squares) and the T0Chg runs (T_0 = 293 and 302 K, triangles and plus marks, respectively) averaged over the second model year. The abscissa is RH_C. The mass flux is defined as the difference between the maximum (in the Northern Hemisphere) and the minimum (in the Southern Hemisphere) of Ψ at 600 hPa in the tropics. Note that RH_C values supported in the T0Chg series are only 0, 0.3, 0.5, 0.7, and 0.9. Furthermore, the value for the run with T_0 = 293 K and RH_C = 0.3 is not shown, since the resultant circulation is highly asymmetric (see text), so a comparison is meaningless.

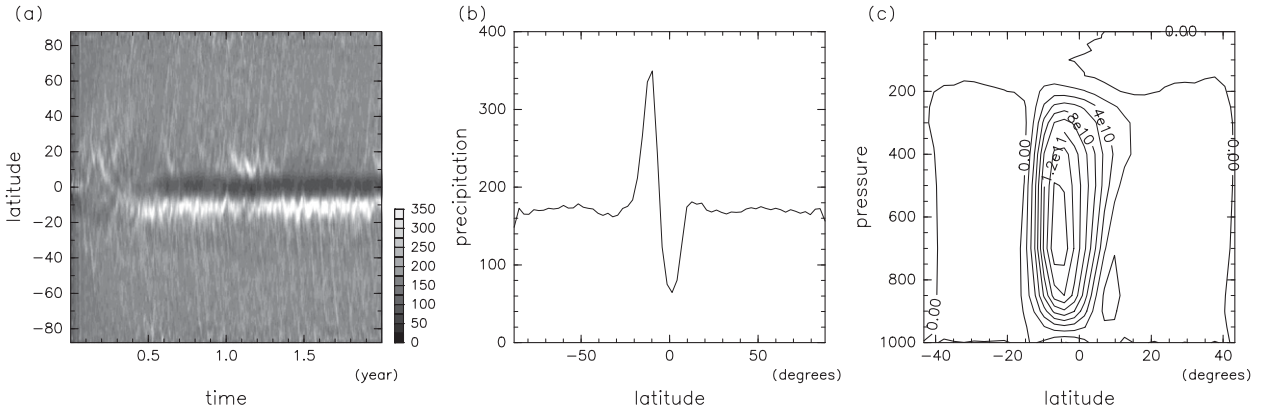

FIG. 5. Results from the run with $RH_C = 0$ in the 4-Col series: (a),(b) precipitation as in Figs. 1 and 2, respectively; (c) mass streamfunction Ψ (kg s^{-1}).

a continuous manner. As mentioned in section 2, RH_C modifies the spatiotemporal variability of tropical precipitation, which is investigated in section 4. For reference, relative humidity thresholds are introduced in many cumulus parameterizations in the course of GCM tuning [e.g., Sud and Walker (1999) in the relaxed Arakawa–Schubert scheme; Zhang et al. (2004) in the Zhang and McFarlane scheme; Li et al. (2007) in the Tiedtke scheme].

Results of the 4-Col series are shown in Fig. 5 for $RH_C = 0$. The only difference between this and the Cntrl series is in radiation, but the resultant mean precipitation and meridional circulation are very different from the ones shown in Figs. 1a–3a. In the 4-Col run, precipitation around 10°S is significantly enhanced, and the corresponding Hadley circulation is asymmetric with a cross-hemispheric mass circulation. The mass flux is comparable to that in the real atmosphere in solstitial seasons, but the width of the circulation is smaller. The off-equatorial precipitation maximum is due to a persistent tropical cyclone circulating zonally to the west off the equator. The result is similar when $RH_C = 0.3$, but the tropical cyclone in a hemisphere disappears at 1.3 model years, and at the same time another appears in the other hemisphere. Therefore, a similar hemispheric flip might occur in the $RH_C = 0$ run too if time integration is extended (not done). At higher RH_C values of 0.7 and 0.9, the tropical cyclone is not formed, and the precipitation is rather equatorially symmetric. The differences between the Cntrl and 4-Col runs are interesting. However, the 4-Col radiation scheme is not tuned, and low-level cloud causes excessive cooling, so this study mainly focuses on the results obtained with the standard radiation scheme.

Chao and Chen (2004) conducted aquaplanet AGCM simulations with globally uniform SST. The cumulus parameterization used is the relaxed Arakawa–Schubert scheme. They found that either an equatorially symmetric or asymmetric ITCZ forms depending on model settings such as in radiation (using a simple uniform cooling or using the model's radiation scheme with or without clouds), surface sensible and latent heat flux (uniformly prescribed or interactively calculated), and RH_C (0 or 0.95). Roughly speaking, the meridional distributions of precipitation in the Cntrl runs with large RH_C are similar to their symmetric cases (although there is a large variation among their results), and those in the 4-Col runs with small RH_C are similar to their asymmetric cases. It is, however, not certain, as it is not mentioned, whether a persistent tropical cyclone is formed in the latter cases of their study.

The contrast between the Cntrl and 4-Col experiments is at least superficially consistent with the result by Raymond (2000) by using a two-dimensional model; since the low-level clouds are denser in the subsidence region, the 4-Col radiation scheme should have a greater cloud–radiation feedback. This issue is revisited in section 6a. Note, however, that a similar circulation can be obtained with the standard radiation scheme, as shown in what follows.

The equatorial precipitation peak in the high RH_C runs in the Cntrl series is much weaker than those obtained by Horinouchi and Yoden (1998) with the moist convective adjustment scheme and by Kirtman and Schneider (2000) with the relaxed Arakawa–Schubert scheme. In these studies, the equatorial precipitation was larger than that in the extratropics by a factor of 2 or more.

In the atmosphere-only experiments by Barsugli et al. (2005), a well-defined equatorially symmetric ITCZ formed with the globally uniform SST values 20° and 30°C, while the zonal mean precipitation was highly transient and the resultant organization of time-mean precipitation was much weaker when SST was 25°C. The

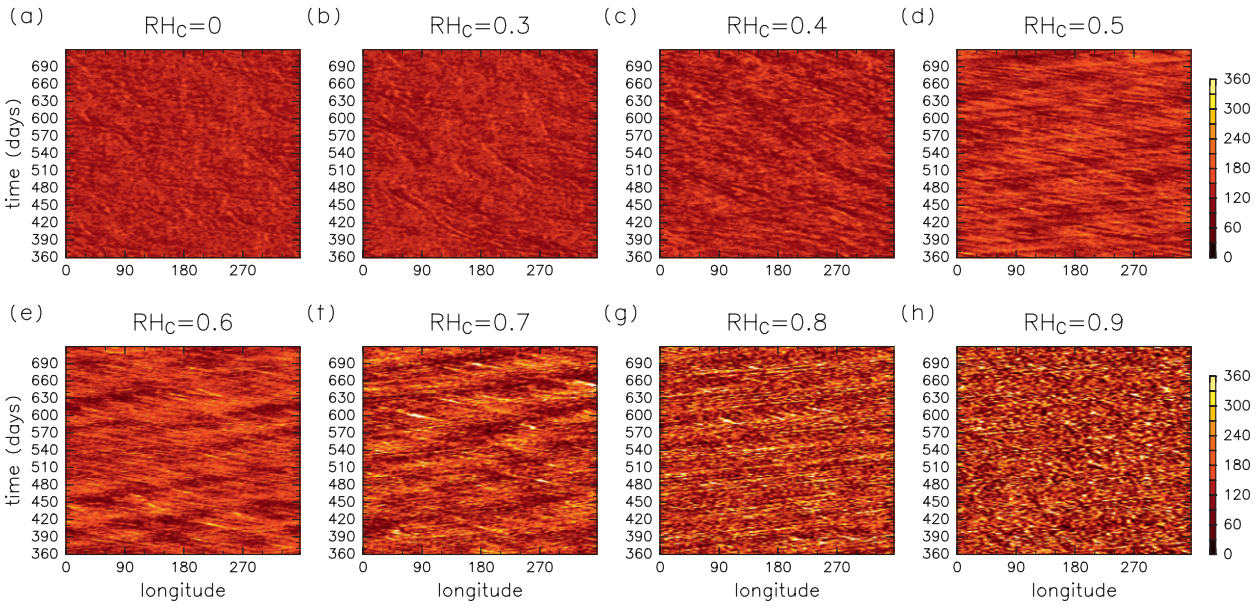

FIG. 6. Longitude–time plots of tropical precipitation averaged between 15°S and 15°N over the second model year of the Cntrl runs (W m^{-2}).

model they used is the National Center for Atmospheric Research Community Climate Model version 3 (CCM3) (with the physics of version 3.6.6), so the cumulus parameterization they used must be the Zhang and McFarlane scheme.

In the current study, dependence on the uniform SST is not like what was in Barsugli et al. As seen in Fig. 4, for $RH_C \geq 0.3$ the strength of the Hadley circulation when $T_0 = 302$ K (~29°C) is quite similar to that when $T_0 = 299$ K (~26°C). The strength is a little weaker when $T_0 = 293$ K (~20°C), but the dependence on RH_C is similar when $RH_C \geq 0.5$.

At $T_0 = 293$ K and $RH_C = 0.3$, the ITCZ and the Hadley circulation are quite similar to those obtained in the 4-Col runs at $RH_C = 0$ and 0.3. This is the only run with the standard radiation scheme in which a distinct asymmetric circulation is formed. However, there could be multiple equilibria for some parameter values, which is not investigated in this study.

4. Possible role of convectively coupled disturbances

a. Control runs

Figure 6 shows longitude–time plots of tropical precipitation in the Cntrl series runs. Variability is larger at $RH_C \geq 0.5$, when well-defined Hadley circulations are formed, than at smaller RH_C values. Both eastward and westward propagating signals are seen there. As RH_C is increased from 0.7 to 0.9, the zonal scales of disturbances become smaller.

Figure 7 shows zonal wavenumber–frequency spectra of tropical precipitation. Signals are enhanced along the dispersion curves of the equatorial waves at the equivalent depth h around 30 m when $RH_C \geq 0.5$. This feature indicates the existence of convectively coupled equatorial waves (Takayabu 1994; Wheeler and Kiladis 1999). Signals corresponding to Kelvin waves and the mixed Rossby–gravity (MRG) waves (or the $n = 0$ eastward-moving inertia gravity waves, which are not distinguished from the MRG waves in this study) are especially evident, while it is difficult to distinguish simple advection and Rossby wave signature from this figure. A similar spectral feature was obtained by Horinouchi and Yoden (1998) in an aquaplanet experiment with globally uniform SST.

It is beyond the scope of this paper to elucidate how RH_C affects the spatiotemporal variability of simulated convection or convectively coupled equatorial waves. However, a few remarks can be made as follows. The relative humidity threshold introduces the convective inhibition to permit the convective available potential energy (CAPE) to be accumulated (e.g., Sud and Walker 1999). Wang and Schlesinger (1999) demonstrated that introduction of this threshold in some cumulus parameterizations can increase the amplitude of the tropical intraseasonal oscillation (ISO). They suggested that this occurs because the need for the accumulation lowers the dominant frequencies of convective precipitation to enhance the intraseasonal time scales. In the present study,

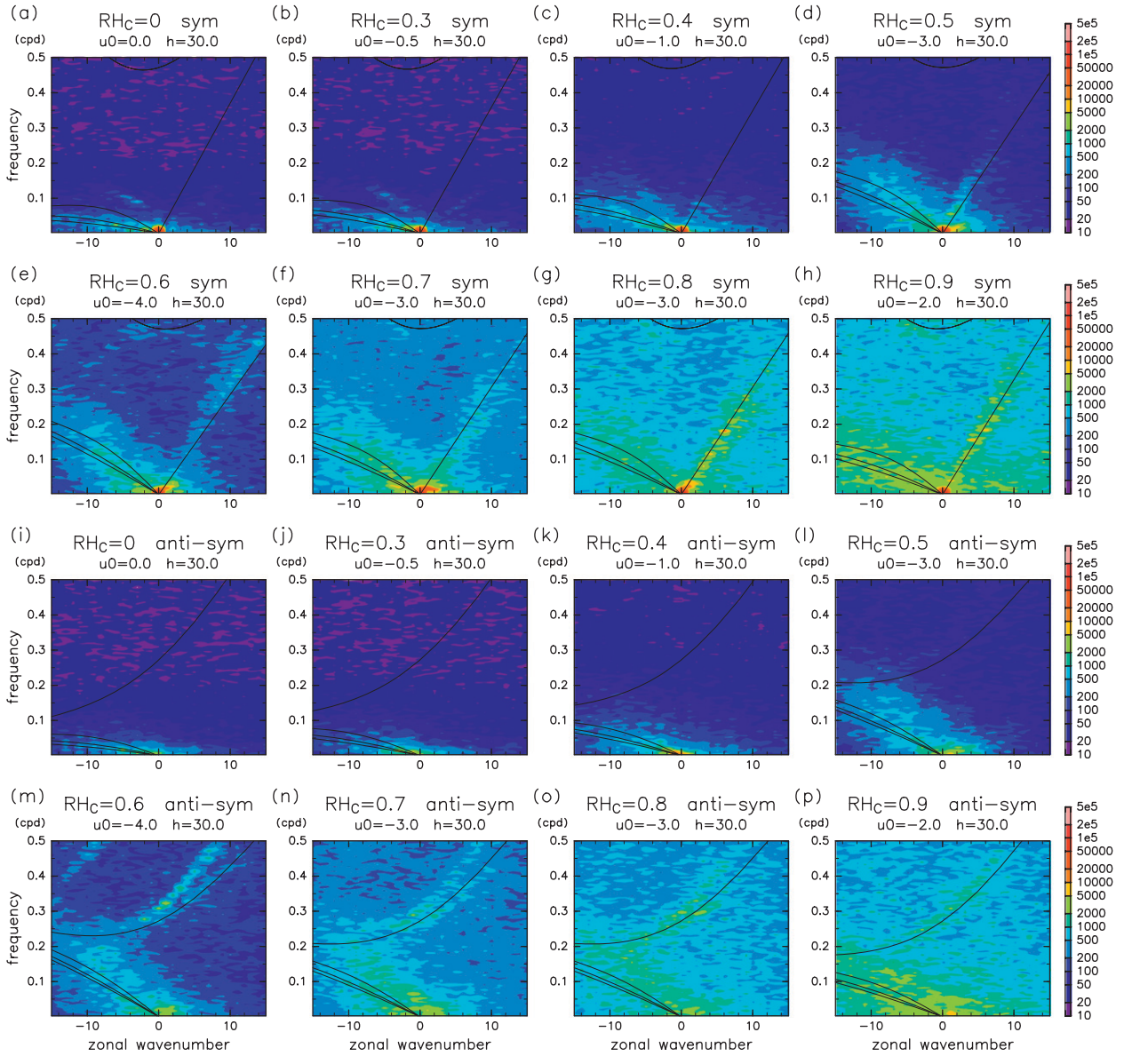

FIG. 7. Zonal wavenumber–frequency spectra of tropical precipitation averaged between 20°S and 20°N derived from the second model year of the Cntrl runs: spectra of (a)–(h) equatorially symmetric and (j)–(p) antisymmetric mode components. Note that coloring is made with a logarithmic scaling. Lines show the dispersion relation of equatorial waves with the equivalent depth $h = 30$ m subject to Doppler shifting with the background zonal velocity at the equator shown above each panel (by "u_0=" m s^{-1}). The values of the background velocity are determined subjectively from mean zonal wind in the equatorial lower troposphere.

a large RH_C caused amplification of the overall convective variability. This may also be attributed to the enhancement of convective inhibition. Note, however, that the relative humidity thresholding is not the only way to control it [e.g., Chikira and Sugiyama (2010); see also Maloney and Hartmann (2001) for ISO simulations]. Therefore, RH_C is regarded in this study as one of the model-dependent parameters that can affect the convective variability.

If a large fraction of tropical precipitation is associated with convectively coupled equatorial waves, it will produce meridional contrast in the distribution of mean precipitation. If averaged over the cycles of waves, convergence and divergence would cancel, but precipitation would not, since it is a nonlinear positive-only quantity. Convergence and divergence associated with low equatorial wave modes occur predominantly near the equator. If $h = 30$ m, the equatorial radius of deformation l_e is

870 km. In the Kelvin waves, convergence and divergence peak at the equator, and the strength falls to $e^{-1/2}$ times at $|y| = l_e$, where $y \equiv R_E\phi$ is the distance from the equator; convergence and divergence of the MRG waves peak at $|y| = l_e$; in the $n = 1$ Rossby waves, the peaks are at $|y| \leq l_e$, but the meridional tails are slightly wider than that of MRG waves. Therefore, the enhancement of precipitation at $y \lesssim 1.5$ seen in Fig. 2 is consistent with the enhancement by convectively coupled equatorial waves.

If precipitation is enhanced in the equatorial region for some reason, precipitation at higher latitudes in the tropics can be suppressed by the formation of subsidence, as discussed in section 6a. Figure 8 shows the relation between the lower-tropospheric perturbation kinetic energy, where the perturbation denotes the deviation from the zonal mean, and the upward mass flux of the Hadley circulation, shown in Fig. 4. Although there is no clear causal relationship between them, the relationship is remarkably compact, perhaps too compact by coincidence. The slope obtained by the least squares fit is 1.19. The relation is rather insensitive to small changes in the latitudinal widths and the vertical extent over which the kinetic energy is averaged. If the energy is, instead, calculated for the upper troposphere, the relationship is still similar but it is slightly less compact and the slope is higher (1.39 if averaged over $200 < p < 600$ hPa).

This result supports, though it does not prove, the suggestion that the convectively coupled equatorial waves play an important role to determine the strength of the simulated Hadley circulation. Note that the circulation is thermally direct, having upwelling where latent heat is released. Therefore, the circulation is not wave-driven.

Convectively coupled equatorial waves play a further role to determine the fine structure of the tropical zonal mean precipitation. Figure 2d shows that tropical precipitation is enhanced right at the equator (actually on the two grid points straddling the equator) when $RH_C = 0.5$. Figures 7d and 7l show that, when $RH_C = 0.5$, convectively coupled Kelvin waves are significant, but convectively coupled MRG waves are weak. This feature is consistent with the narrow peak at the equator. When RH_C is 0.6–0.8, on the other hand, the tropical precipitation is enhanced over a wider latitudinal range, and secondary peaks are found at the grid points at $|\phi| \sim 7°$ (Fig. 2). In this RH_C range, both Kelvin and MRG waves are significant (Fig. 7). This is also consistent with the distribution of tropical precipitation. When $RH_C = 0.9$, the signature of MRG waves is also evident, and slow westward-moving spectral power, which might be partly associated with Rossby waves, is relatively strong. This feature could be consistent with the tropical precipitation structure in Fig. 2h, which is smoother than that with smaller RH_C values.

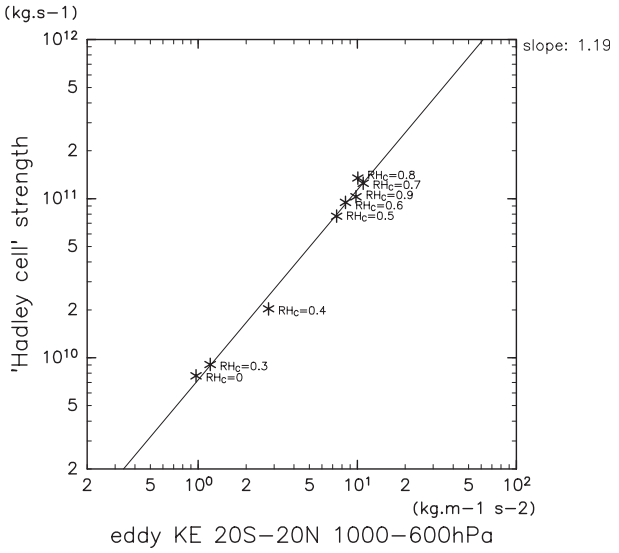

FIG. 8. Relation between the lower-tropospheric perturbation kinetic energy (kinetic energy of the deviation from the zonal mean horizontal winds averaged between 20°S and 20°N and $600 \leq p \leq 1000$ hPa) and the upward mass flux of the Hadley circulation $\Delta\Psi_{600}$ for the Cntrl series. The line shows the least squares fit.

b. Restricting equatorial disturbances

Further investigation is made to elucidate the possible roles of convectively coupled equatorial waves. Figure 9 shows the mean precipitation and mass streamfunction from the Eqdmp run. In this run, the Rayleigh friction with a time scale of 2 days is applied to the perturbation horizontal winds between 10°N and 10°S. The resultant Hadley circulation is weaker, and the contrast in the tropical precipitation is smaller than in the corresponding Cntrl run with $RH_C = 0.7$. This is expected if convectively coupled equatorial waves play an important role in the formation the Hadley circulation in the Cntrl run. However, precipitation minima still exist around $|\phi| \sim 20°$, and the Hadley circulation did not vanish. In this run, equatorial precipitation varied nearly axisymmetrically, but transient disturbances did not disappear. The dominant variation is a zonal wavenumber-0, equatorially antisymmetric oscillation with a period of 4 days, as can be seen in Fig. 9a at close look. The oscillation is consistent with the zonal wavenumber-0 MRG wave with $h \sim 20$ m. It is not clear to what extent the subtropical weak rainfall suppression can be attributed to the transient disturbances.

Figure 10 shows the result from the Axsym run. The mean precipitation shows narrow peaks and depressions around the two tropics (Fig. 10c). The meridional streamfunction shows corresponding narrow peaks (Fig. 10b). Note that transient variability is evident in this run too (Fig. 10a). Kirtman and Schneider (2000) showed that transient variability dominates the momentum transport

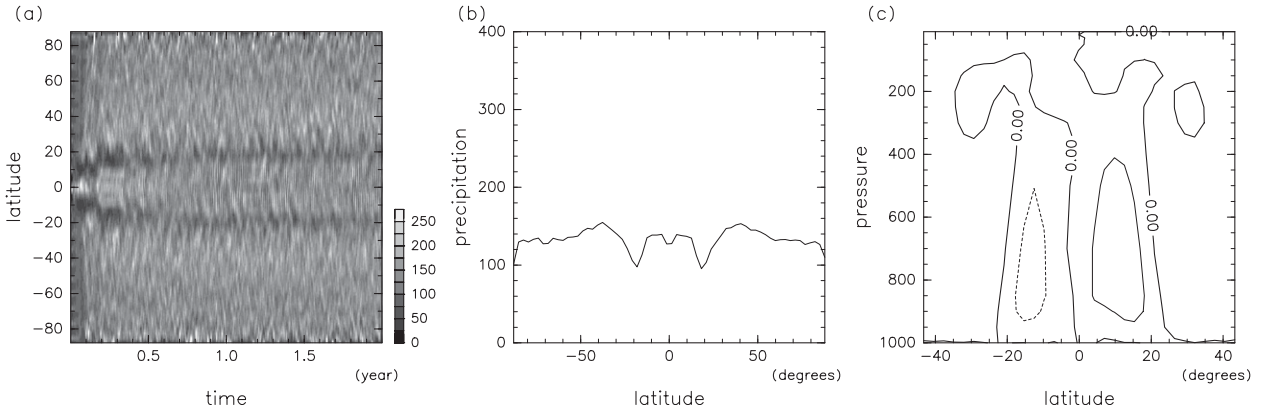

FIG. 9. As in Fig. 5, but for the Eqdmp run.

in the tropical lower troposphere in their axisymmetric run, although the variability is at much lower frequencies than in the present study. See also Satoh (1995) for axisymmetric aquaplanet experiments.

Axisymmetric runs exclude not only convectively coupled nonzero wavenumber waves but also other disturbances that can redistribute angular momentum. Therefore, investigating this run is not very fruitful in the current context of the study (see section 6b for discussion on angular momentum).

c. *Changing the rotation rate*

In the RotChg series, the planetary rotation rate is changed to ½ and ¼ times the earth's rotation rate. The resultant time evolution of zonal mean precipitation is shown in Fig. 11. The width of enhanced precipitation in the ITCZ is approximately doubled when the rotation rate is 4 times slower. This result is consistent with the change in l_e, which is proportional to $\Omega^{-1/2}$. Thus, the result is not inconsistent with the importance of convectively coupled equatorial waves.

However, there could be other factors that also vary in proportion to $\Omega^{-1/2}$. For instance, the critical latitude at which the baroclinic instability shown in the next section is initiated can also be proportional to $\Omega^{-1/2}$ in the equatorial β plane. Also, when dealing with such scaling lows, one should be aware of possible limitation of the equatorial β-plane approximation. Its validity is a prerequisite for a simple meridional scaling low to hold. This may not be granted if the phenomena of interest extend well into the extratropics.

5. Effect of nonuniform SST

The importance of convectively coupled equatorial waves was shown in section 4 using the experiments with globally uniform SST. This feature is dynamically supported by the high degree of freedom in the meridional distribution of convective heating as shown in section 6a and the passive angular momentum redistribution as shown in section 6b. However, the occurrence of penetrative convection is affected by gross moist stability. It

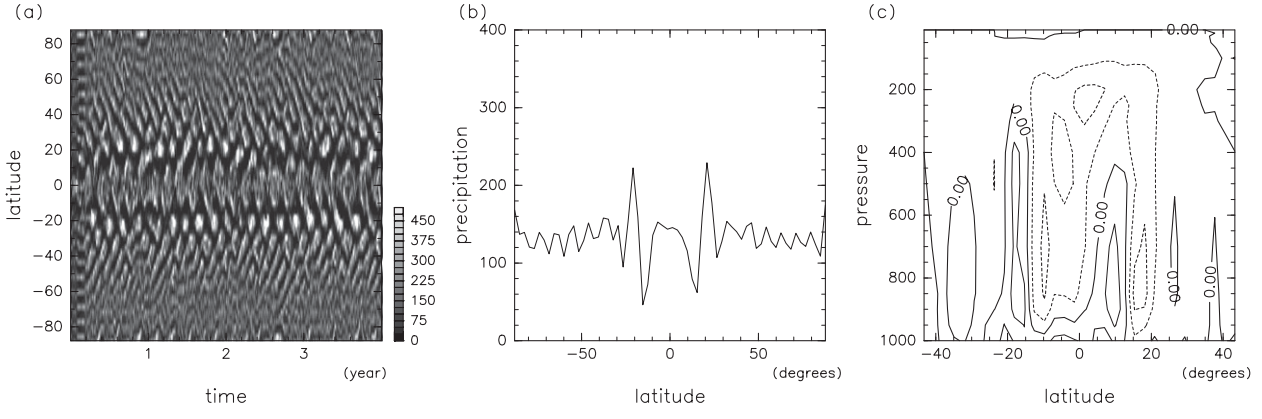

FIG. 10. As in Fig. 5, but for the Axsym run.

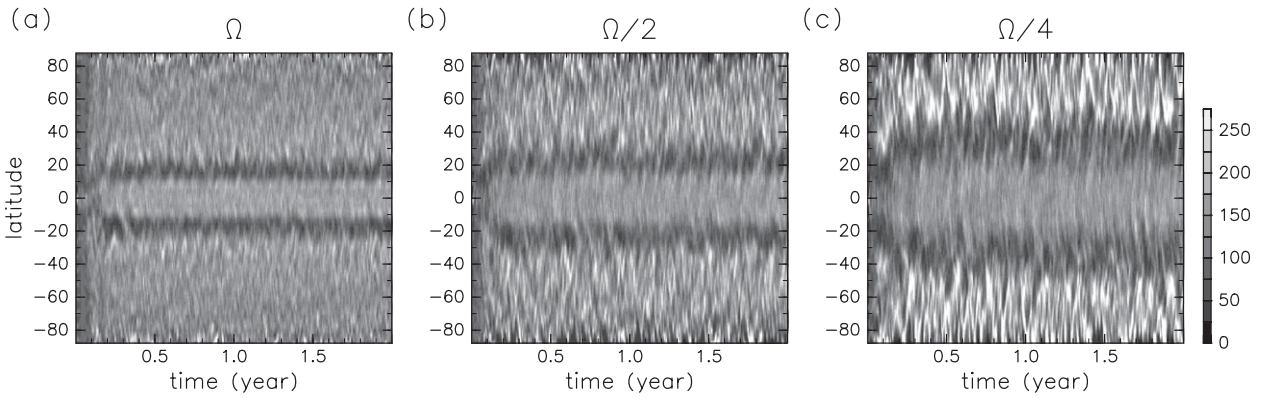

FIG. 11. As in Fig. 1, but for the RotChg series.

depends on subcloud moist static energy, which is affected, if not dominated, by SST. Therefore, it is questioned to what extent the mechanisms working in the uniform SST experiments work if SST is not uniform. Here investigation is made on the effect of SST variation by introducing a simple meridional dependence decreasing toward the poles.

Figure 12 shows the meridional distribution of precipitation obtained in the Y2-eq and Y2–10N series. As Δ_S is increased, precipitation around the SST peak is increased. At the same time, width of the suppressed region, associated with subsidence, is increased. The increase in the poleward extent of the subsidence region may partly be explained by the poleward shift of the baroclinic instability suggested in section 6b. This is because the local thermal wind outside the meridional circulation is increased as the meridional SST gradient is increased. However, as Δ_S is increased, the familiar baroclinic instability owing to the surface baroclinicity takes over, so the mechanism suggested above was not successfully isolated by data analysis.

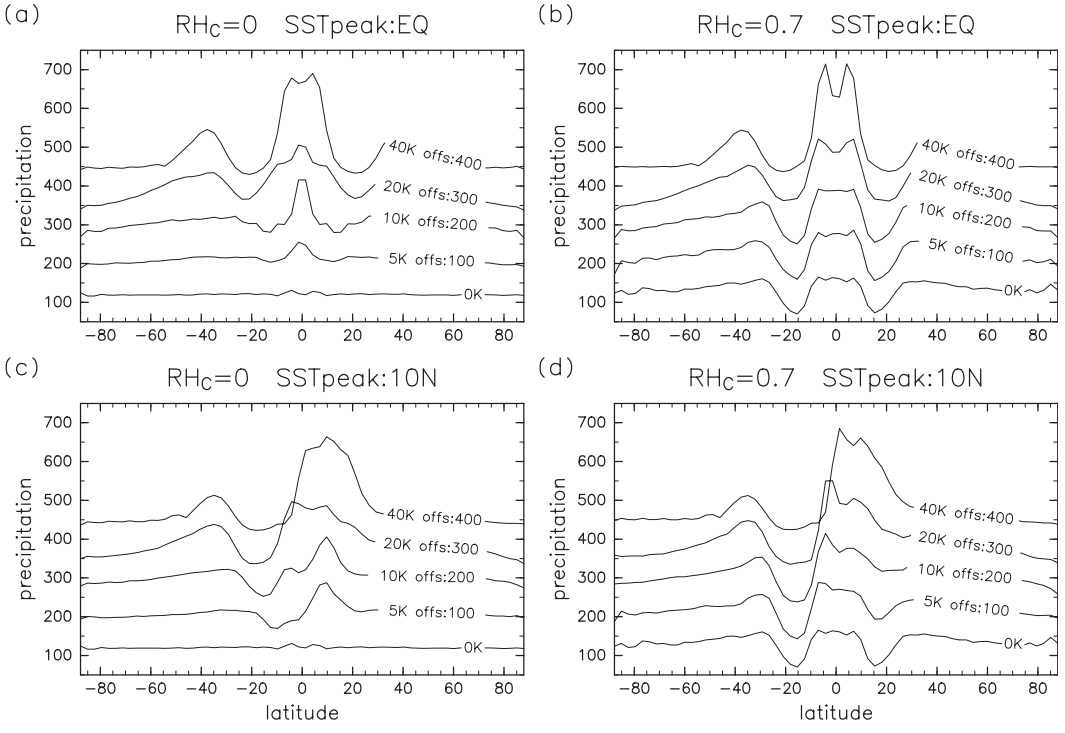

FIG. 12. Meridional distribution of precipitation averaged over the second model year in the (a),(b) Y2-eq and (c),(d) Y2–10N series when RH_C is (left) 0 and (right) 0.7. In each panel results for Δ_S = 0, 5, 10, 20, and 40 K are shown, with offsets of 0, 100, 200, 300, and 400 W m^{-2}, respectively, for illustration purposes.

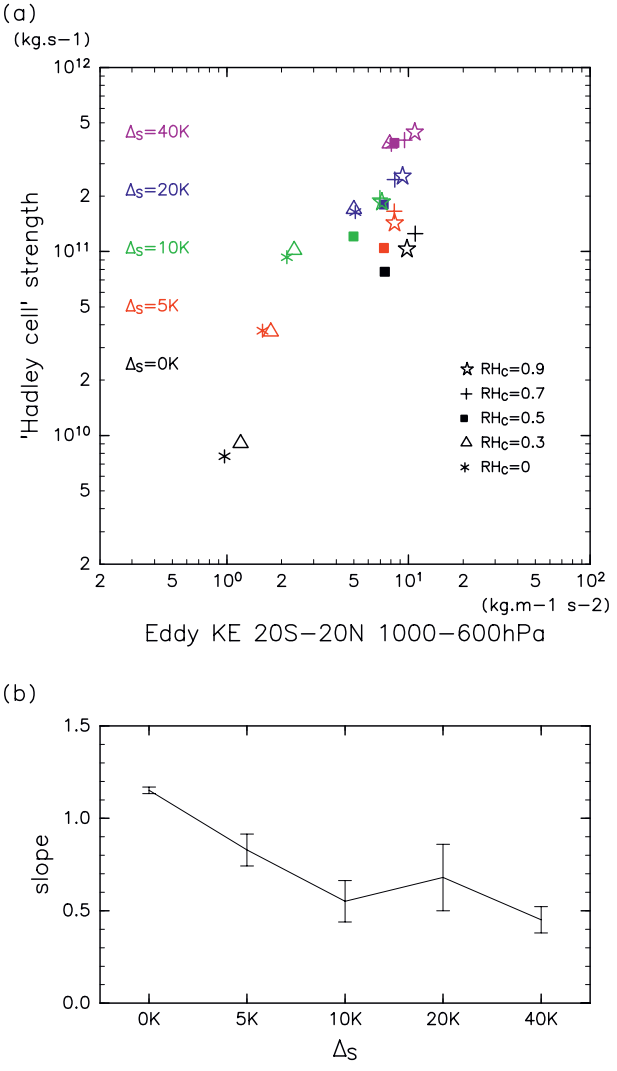

FIG. 13. (a) As in Fig. 8, but for the Y2-eq series. The RH_C values are indicated by different symbols; Δ_S values by colors. (b) Slope of the linear least squares fit for each Δ_S value based on the log–log scaling in (a). Standard errors are shown by the error bars.

Figure 13a shows the relation between the lower-tropospheric perturbation kinetic energy and upward mass flux of the Hadley circulation for the Y2-eq series. Sensitivity of both parameters to RH_C decreases as Δ_S is increased. At $\Delta_S = 40$ K the difference in the kinetic energy is within a factor of 1.4. However, the positive correlation between kinetic energy and the Hadley circulation strength is retained. The slope in the log–log scaling is shown in Fig. 13b for each Δ_S value. As expected from the increasing contribution from the SST gradient, the slope is decreased as Δ_S is increased. However, the value remains at ~0.5. This result suggests that the dependence of the Hadley circulation strength on the tropical disturbances remains at realistic pole–equator SST gradients. However, since the dynamic range of the kinetic energy is not large at $\Delta_S = 40$ K, further investigation would be desirable. That would require a sensitivity study that is not within the current experimental design, so it is left for future studies.

In section 4 it is shown that the convectively coupled equatorial waves leave clear signatures in the fine structures of the simulated ITCZs when $\Delta_S = 0$. The relation is also seen when $\Delta_S \neq 0$. As in the cases with $\Delta_S = 0$ described in section 4, some of the simulated ITCZ have equatorial sharp peaks while some have peaks off the equator. Zonal wavenumber–frequency spectra of tropical precipitation as shown in Fig. 7 are examined for nonzero Δ_S too (not shown), and it is found that the correspondence between ITCZ structure and the dominant convectively coupled equatorial wave signals hold even when $\Delta_S > 0$. More specifically, for both series when $\Delta_S =$ 5, 10, or 20 K, the MRG wave signals are weak if $RH_C =$ 0 and are evident when $RH_C = 0.7$. As for the cases with $\Delta_S = 40$ K, a clear explanation was not found, but for both $RH_C = 0$ and 0.7, low-frequency westward signals exhibited relatively high power, so this could explain the meridional structures.

It is noteworthy that in the Y2–10N series the meridional distribution of precipitation does not follow the SST increase in the Northern Hemisphere. The maximum is in the Southern Hemisphere when $RH_C = 0.7$ and $\Delta_S \leq 20$ K. This behavior may be supported by the convectively coupled equatorial waves.

6. Discussion

a. *Thermodynamic constraints*

The results shown above, along with the past studies mentioned above, suggest that the strength of the ITCZ and Hadley circulation is quite variable and depends on subtle model setups such as a tunable parameter in the cumulus parameterization. The existence of the circulation cannot be explained by the HH theory, so a discussion is made here.

If the horizontal transport of dry static energy s is neglected, which can be justified to the first approximation in the tropical free troposphere (Sobel et al. 2001), and if the surface sensible heating neglected as being small, the steady-state vertically averaged thermodynamic energy equation for a single column can be expressed as

$$-\sigma\omega = -R + C, \tag{4}$$

where ω is the column-mean pressure velocity, σ is a positive parameter on the static stability, and R and C are the column-mean radiative cooling and condensation heating, respectively.

Under the persistent presence of penetrative deep convection somewhere in the tropics, the vertical thermodynamic structure approaches the moist adiabat. Therefore, to the first approximation, the radiative cooling rate R can be regarded as a constant, say R_0, throughout the tropics. If the mass circulation is closed within a region of the tropical meridional circulation, the domain averaged C is simply equal to R_0. Then, ω in the region of subsidence can have any value between 0 and $\sigma^{-1}R_0$ depending on the inhomogeneity in C. Since the distribution of cumulus convection can be interactively adjusted while a meridional circulation is formed, a meridional circulation is possible even when the SST is uniform. This is a fundamental difference of a moist atmosphere from a Newtonian-cooling driven atmosphere in which diabatic heating is strongly tied to temperature. Note that C is the net column condensation heating. If the convective adjustment is a dry one [or if it does not provide net column heating as in Walker and Schneider (2006)], the adjustable nature mentioned above does not exist. Therefore, the thermodynamic framework of HH may still be appropriate to a dry radiative–convective atmosphere, such as on Mars.

Condensation heating must also satisfy the steady-state moisture budget. If the Hadley circulation is the only dynamical feature that exists in the system considered, the moisture budget may introduce another constraint to predict the circulation given SST. However, the three-dimensional moist atmosphere can have transient disturbances, which are affected by factors other than SST (specifically, RH_C in the experiments of this study). Since they introduce a new degree of freedom, the moisture budget does not necessarily provide a good constraint. An analysis conducted in this study showed that eddy moisture transport is indeed significant in the moisture budget of many of the experiments (not shown). However, insight beyond that was not obtained since the difference among the experiments did not appear systematic. Raymond (2000) demonstrated that the cloud–radiation feedback can significantly affect the Hadley circulation in an axisymmetric model [see also Bretherton and Sobel (2002) for the study on the Walker circulation]. However, the new degree of freedom associated with transient disturbances can also be important (and can even be more important).

b. Angular momentum budget

Meridional temperature structure is associated with zonal wind through the thermal wind relationship. HH showed that, if the absolute angular momentum around the earth's rotation axis is conserved along the poleward branch of the Hadley circulation, vertically averaged temperature decreases with latitude proportional to y^4. If SST is uniform, atmospheric temperature near the surface

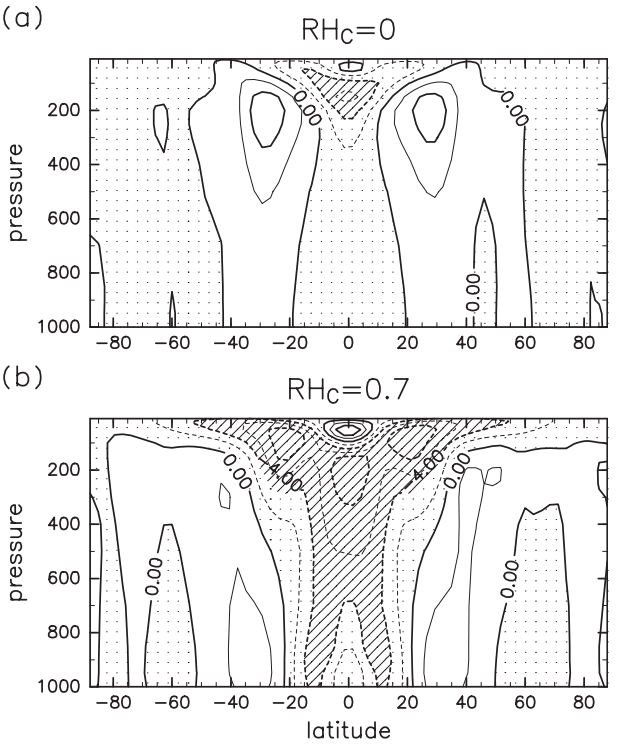

FIG. 14. Mean zonal wind averaged over the second model year in the Cntrl runs with RH_C = (a) 0 and (b) 0.7. Contour interval = 2 m s^{-1}. Negative values are shaded.

is also nearly uniform. In this case, the static stability would decrease with latitude since the temperature aloft must decrease to accomplish the decrease in the vertical average. Therefore, if the circulation is axisymmetric and nearly inviscid, there exists a negative feedback in the moist atmosphere to suppress the formation of the (at least near symmetric) ITCZ.

In the Cntrl runs, however, the angular momentum is not conserved along the poleward branch of the Hadley circulation as shown in Fig. 3. Actually, zonal wind is quite weak as shown in Fig. 14, so the angular momentum is dominated by the planetary rotation.

Is the angular momentum change along the upper branch induced by the convectively coupled equatorial waves? If the answer is yes, one can say that the simulated Hadley circulation is created self-consistently by the waves. However, the answer is no, as shown in what follows.

The steady-state angular momentum budget is expressed in the standard notation of the log-pressure coordinate system (see Andrews et al. 1987) as

$$\overline{u}^{*}\frac{\partial \overline{m}}{\partial \phi} + \overline{w}^{*}\frac{\partial \overline{m}}{\partial z} = \rho_0^{-1}\nabla \cdot \mathbf{F} + \overline{X}. \qquad (5)$$

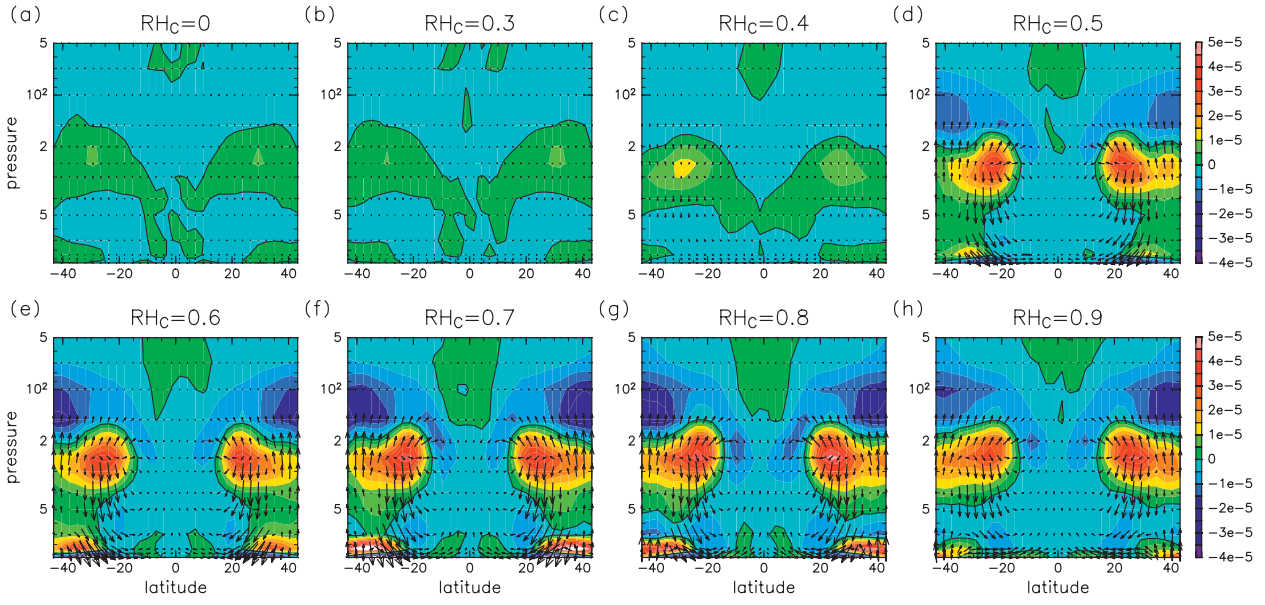

FIG. 15. The EP flux **F** (arrows) and $\rho_0^{-1}\nabla \cdot \mathbf{F}$ (shading) averaged over the second model year of the Cntrl runs. The divergence is multiplied by a constant factor to make the units in m s^{-2}. Unlike the other figures, the ordinate p is shown with a logarithmic scaling. The contour is plotted where the value is zero.

Thus, the angular momentum change along the meridional circulation is associated with divergence of the Eliassen–Palm (EP) flux **F**. The frictional term $\overline{X}$ is negligible in the free troposphere. Here, $\overline{v}^*$ and $\overline{w}^*$ are the transformed Eulerian mean residual circulation rather than the naive Eulerian mean circulation shown in Fig. 3. However, it is confirmed for the Cntrl runs that the difference is small in the Hadley circulation region (not shown). On the other hand, the simulated ''Ferrel'' circulation is rather stronger in the residual circulation than in Eulerian circulation, suggesting that the direction of the meridional Stokes drift is opposite to that in the real atmosphere.

The EP flux and its divergence in the Cntrl runs are shown in Fig. 15. A convergence (in bluish colors) is found in the upper troposphere within the Hadley circulation. This is consistent with the angular momentum decrease along the poleward branch. The EP flux that caused this convergence comes from higher latitudes. A further analysis (not shown) is made to confirm that the flux is associated with intrinsically westward-moving disturbances, so the direction of arrows represents that of the group propagation.

The EP flux from higher latitudes (at ~30°) is likely due to baroclinic instability in the interior of the upper troposphere. The mechanism is illustrated in Fig. 16. Without contributions from eddies, steady-state thermal-wind-balanced zonal wind outside the meridional circulation is zero if SST and solar insolation are uniform. Therefore, if the upper branch of the meridional circulation conserves angular momentum, a shear (or a discontinuity in zonal wind if the system is inviscid) will develop at the poleward boundary of the circulation. The shear is cyclonic, so the potential vorticity there has a positive anomaly. If it is strong enough, the meridional potential vorticity gradient is negative on its poleward flank. Therefore, it is unstable to cause stirring. The actual latitudes at which the unstable disturbances develop in simulations depend on the zonal wind at the equator u_{eq} and the model resolution. It was confirmed that the contribution of the model horizontal hyperdiffusion was negligible.

The mechanism proposed above is passive to the meridional circulation. Thus, it is understood that the EP flux convergence/divergence was larger in the runs in which the meridional circulation was stronger. Also, this mechanism does not occur in axisymmetric runs. This is the reason that the Eqdmp run is more suitable than the Axsym run for the purpose of comparing with the Cntrl runs.

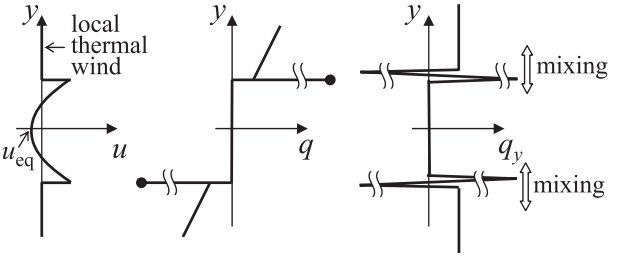

FIG. 16. Schematic illustration of how the baroclinic/barotropic instability occurs in the upper troposphere: u and q represent zonal mean zonal wind and potential vorticity, respectively; u_{eq} is the zonal wind at the equator. See text for the mechanism explanation.

If the meridional gradient exists in SST, the baroclinic instability owing to the surface baroclinicity can also present. That can also affect the width of the Hadley circulation. The relative importance of the two types of baroclinic instability depending on Δ_S is left unrevealed in this study.

7. Summary and conclusions

Aquaplanet simulations have been conducted to advance our understanding and the numerical modeling of the Hadley circulation and the ITCZ for given SST. Possible roles of transient tropical disturbances have been investigated.

In the control series, SST is set uniformly to 299 K, and the relative humidity threshold of the model's cumulus parameterization RH_C is varied. Depending on the threshold value, features like the ITCZ and the Hadley circulation that are nearly symmetric with respect to the equator emerge spontaneously. The strength of the circulation is increased as the value of RH_C is increased from 0 to 0.8 by more than 10 times, and it is slightly decreased when RH_C is further increased to 0.9. The largest strength is greater than the half of the observed climatological mass flux in the real atmosphere in the equinoctial seasons. The width of each of the Hadley cells is about 20° irrespective of the values of RH_C, which is smaller than in the real atmosphere. When the radiation scheme is changed to a simple four-color scheme, which causes excessive cooling by low-level clouds, and when RH_C is small, an equatorially asymmetric Hadley circulation is obtained. This circulation is associated with a long-lived tropical cyclone. A similar case is found with the standard radiation scheme, when the prescribed uniform SST is 293 K and $RH_C = 0.3$.

In the control series, the spatiotemporal variability of tropical precipitation is large in the runs with large $RH_C \geq 0.5$ in which well-defined ITCZs and Hadley circulations formed. In this case, spatiotemporal spectra of tropical precipitation exhibited clear signatures of convectively coupled equatorial waves whose equivalent depths h are around 30 m.

The waves can cause the concentration of precipitation to the equatorial region. If averaged over the cycles of waves, convergence and divergence would cancel, but precipitation would not, since it is a nonlinear positive-only quantity. The meridional scales of the low equatorial wave modes of $h \sim 30$ m are consistent with the meridional extent of the enhanced precipitation. Moreover, the fine structure of the ITCZ in each run is consistent with the meridional structure of convergence field associated with dominant equatorial waves. It is found that the strength of the simulated Hadley circulation has a high correlation with the eddy kinetic energy in the tropical lower troposphere. If an additional Rayleigh damping is introduced on perturbation horizontal winds in the equatorial regions, the Hadley circulation was weakened. If the planetary rotation rate is changed to 4 times slower, the width of enhanced precipitation in the ITCZ is approximately doubled, consistent with the Ω dependence of the equatorial radius of deformation. These results suggest the importance of convectively coupled equatorial waves in the simulated ITCZ and Hadley circulation.

Simulations are also conducted with SST decreasing toward the poles, where the pole-to-equator SST difference is characterized by the parameter Δ_S. As Δ_S is increased for given RH_C, precipitation is more concentrated to around the SST peaks, and the meridional circulation is strengthened, as expected in terms of the SST control on the Hadley circulation. For given Δ_S, however, there still remains a tendency that the circulation is stronger if the lower-tropospheric eddy kinetic energy is greater, where the slope of the linear regression shown in Fig. 13b remained around 0.5. Therefore, convectively coupled waves are likely to play a role in the runs with nonuniform SST. It is also noteworthy that the fine structures of the ITCZs are consistent with the meridional structure of the dominant equatorial waves even at nonzero Δ_S.

Discussion is made on the fundamental differences in the thermodynamic constraints between moist convective atmospheres and radiatively driven, or dry convective, atmospheres. It elucidates that, in an atmosphere in which convection releases net latent heat release, the distribution of convective heating can be interactively adjusted while a circulation is formed. This adjustable nature is the source of the large variability in the Hadley circulation strength when the SST gradient is weak.

Also discussed is the angular momentum budget. If the poleward branch of the circulation conserves the angular momentum around the rotation axis, a negative feedback exists to suppress formation of the ITCZ since the thermal wind balance implies that the static stability is decreased as the distance from the equator is increased. However, the angular momentum is effectively reduced while being advected in the poleward branch, so the feedback does not work. It is accomplished by baroclinic instability within the upper troposphere when the SST gradient is weak.

This study shows that SST does not necessarily dominate the ITCZ and Hadley circulation when the SST gradient is weak. Convectively coupled equatorial waves affect the concentration of precipitation to the equatorial region and furthermore the internal structure of the ITCZ. Their roles have not drawn much attention in the context of the climatology of the ITCZ and Hadley

circulation. However, they might be important in the real atmosphere, and also they can affect climate predictions by numerical modeling. In numerical models, the waves are greatly affected by cumulus parameterization. For better climate modeling and understanding, further studies would be needed to establish the relationship among cumulus parameterization, transient disturbances, and tropical circulation.

Acknowledgments. The author thanks two anonymous reviewers for their valuable comments. This study is supported in part by JSPS Grants 22540444 and 20244076. The CCSR/NIES/FRCGC AGCM was developed mainly at University of Tokyo, National Institute for Environmental Studies, and Japan Agency for Marine-Earth Science and Technology. Data analysis and visualization are made using the GFD-Dennou Ruby libraries.

REFERENCES

Andrews, D. G., J. R. Holton, and C. B. Leovy, 1987: *Middle Atmosphere Dynamics*. Academic Press, 489 pp.

Back, L. E., and C. S. Bretherton, 2009: On the relationship between SST gradients, boundary layer winds, and convergence over the tropical oceans. *J. Climate,* **22,** 4182–4196.

Barsugli, J., S.-I. Shin, and P. D. Sardeshmukh, 2005: Tropical climate regimes and global climate sensitivity in a simple setting. *J. Atmos. Sci.,* **62,** 1226–1240.

Becker, E., G. Schmitz, and R. Geprags, 1997: The feedback of midlatitude waves onto the Hadley cell in a simple general circulation model. *Tellus,* **49A,** 182–199.

Bellon, G., and A. H. Sobel, 2010: Multiple equilibria of the Hadley circulation in an intermediate-complexity axisymmetric model. *J. Climate,* **23,** 1760–1778.

Biasutti, M., A. H. Sobel, and Y. Kushnir, 2006: AGCM precipitation biases in the tropical Atlantic. *J. Climate,* **19,** 935–958.

Bretherton, C. S., 2007: Challenges in numerical modeling of tropical circulations. *The Global Circulation of the Atmosphere,* T. Schneider and A. H. Sobel, Eds., Princeton University Press, 302–330.

——, and A. H. Sobel, 2002: A simple model of a convectively coupled Walker circulation using the weak temperature gradient approximation. *J. Climate,* **15,** 2907–2920.

Chao, W. C., and B. Chen, 2004: Single and double ITCZ in an aqua-planet model with constant sea surface temperature and solar angle. *Climate Dyn.,* **22,** 447–459.

Charney, J. G., 1971: Tropical cyclogenesis and the formation of the intertropical convergence zone: Mathematical problems in geophysical fluid dynamics. *Mathematical Problems of Geophysical Fluid Dynamics,* Vol. 13, *Lectures in Applied Mathematics,* American Mathematical Society, 355–368.

Chikira, M., and M. Sugiyama, 2010: A cumulus parameterization with state-dependent entrainment rate. Part I: Description and sensitivity to temperature and humidity profiles. *J. Atmos. Sci.,* **67,** 2171–2193.

Emori, S., A. Hasegawa, T. Suzuki, and K. Dairaku, 2005: Validation, parameterization dependence, and future projection of daily precipitation simulated with a high-resolution atmospheric GCM. *Geophys. Res. Lett.,* **32,** L06708, doi:10.1029/2004GL022306.

Gregory, D., and M. J. Miller, 1989: A numerical study of the parametrization of deep tropical convection. *Quart. J. Roy. Meteor. Soc.,* **115,** 1209–1241.

Gu, G. J., and C. D. Zhang, 2002: Westward-propagating synoptic-scale disturbances and the ITCZ. *J. Atmos. Sci.,* **59,** 1062–1075.

Hasumi, H., and S. Emori, Eds., 2004: K-1 coupled GCM (MIROC) description. K-1 Tech. Rep. 1, Center for Climate System Research, University of Tokyo, 34 pp. [Available online at http://www.ccsr.u-tokyo.ac.jp/kyosei/hasumi/MIROC/tech-repo.pdf.]

Held, I. M., and A. Y. Hou, 1980: Nonlinear axially symmetric circulations in a nearly inviscid atmosphere. *J. Atmos. Sci.,* **37,** 515–533.

Hess, P. G., D. S. Battisti, and P. J. Rasch, 1993: Maintenance of the intertropical convergence zones and the large-scale tropical circulation on a water-covered earth. *J. Atmos. Sci.,* **50,** 691–713.

Holton, J. R., J. M. Wallace, and J. A. Young, 1971: On boundary layer dynamics and the ITCZ. *J. Atmos. Sci.,* **28,** 275–280.

Horinouchi, T., and S. Yoden, 1998: Wave–mean flow interaction associated with a QBO-like oscillation simulated in a simplified GCM. *J. Atmos. Sci.,* **55,** 502–526.

Kirtman, B. P., and E. K. Schneider, 2000: A spontaneously generated tropical atmospheric general circulation. *J. Atmos. Sci.,* **57,** 2080–2093.

Li, L. J., B. Wang, Y. Q. Wang, and H. Wang, 2007: Improvements in climate simulation with modifications to the Tiedtke convective parameterization in the grid-point atmospheric model of IAP LASG (GAMIL). *Adv. Atmos. Sci.,* **24,** 323–335.

Lin, J.-L., 2007: The double-ITCZ problem in IPCC AR4 coupled GCMs: Ocean–atmosphere feedback analysis. *J. Climate,* **20,** 4497–4525.

Lindzen, R. S., and S. Nigam, 1987: On the role of sea surface temperature gradients in forcing the low-level winds and convergence in the tropics. *J. Atmos. Sci.,* **44,** 2418–2436.

——, and A. Y. Hou, 1988: Hadley circulations for zonally averaged heating centered off the equator. *J. Atmos. Sci.,* **45,** 2416–2427.

Maloney, E. D., and D. L. Hartmann, 2001: The sensitivity of intraseasonal variability in the NCAR CCM3 to changes in convective parameterization. *J. Climate,* **14,** 2015–2034.

Nakajima, T., M. Tsukamoto, Y. Tsushima, A. Numaguti, and T. Kimura, 2000: Modelling of the radiative process in an atmospheric general circulation model. *Appl. Opt.,* **39,** 4869–4878.

Numaguti, A., 1993: Dynamics and energy balance of the Hadley circulation and the tropical precipitation zones—Significance of the distribution of evaporation. *J. Atmos. Sci.,* **50,** 1874–1887.

Raymond, D. J., 2000: The Hadley circulation as a radiative–convective instability. *J. Atmos. Sci.,* **57,** 1286–1297.

Satoh, M., 1995: Hadley circulations and large-scale motions of moist convection in the two-dimensional numerical model. *J. Meteor. Soc. Japan,* **73,** 1059–1078.

——, M. Shiobara, and M. Takahashi, 1995: Hadley circulations and their roles in the global angular-momentum budget in two- and three-dimensional models. *Tellus,* **47A,** 548–560.

Schneider, E. K., 1984: Response of the annual and zonal mean winds and temperatures to variation in the heat and momentum sources. *J. Atmos. Sci.,* **41,** 1093–1115.

Sobel, A. H., J. Nilsson, and L. M. Polvani, 2001: The weak temperature gradient approximation and balanced tropical moisture waves. *J. Atmos. Sci.,* **58,** 3650–3665.

Sud, Y. C., and G. K. Walker, 1999: Microphysics of clouds with the relaxed Arakawa–Schubert scheme (McRAS). Part I: Design

and evaluation with GATE Phase III data. *J. Atmos. Sci.,* **56,** 3196–3220.

Sumi, A., 1992: Pattern formation of convective activity over the aqua-planet with globally uniform sea surface temperature (SST). *J. Meteor. Soc. Japan,* **70,** 855–876.

Takayabu, Y. N., 1994: Large-scale cloud disturbances associated with equatorial waves. Part I: Spectral features of the cloud disturbances. *J. Meteor. Soc. Japan,* **72,** 433–449.

Walker, C. C., and T. Schneider, 2006: Eddy influences on Hadley circulations: Simulations with an idealized GCM. *J. Atmos. Sci.,* **63,** 3333–3350.

Wang, W., and M. E. Schlesinger, 1999: The dependence on convection parameterization of the tropical intraseasonal oscillation simulated by the UIUC 11-layer atmospheric GCM. *J. Climate,* **12,** 1423–1457.

Wheeler, M., and G. N. Kiladis, 1999: Convectively coupled equatorial waves: Analysis of clouds and temperature in the wavenumber–frequency domain. *J. Atmos. Sci.,* **56,** 374–399.

Xie, S.-P., 2005: The shape of continents, air–sea interaction, and the rising branch of the Hadley circulation. *The Hadley Circulation: Present, Past and Future,* H. Diaz and R. Bradley, Eds., Cambridge University Press, 489–511.

——, and S. G. H. Philander, 1994: A coupled ocean-atmosphere model of relevance to the ITCZ in the eastern Pacific. *Tellus,* **46A,** 340–350.

Zhang, C., M. McGauley, and N. A. Bond, 2004: Shallow meridional circulation in the tropical eastern Pacific. *J. Climate,* **17,** 133–139.

Zhang, G. J., and M. Mu, 2005: Effects of modifications to the Zhang–McFarlane convection parameterization on the simulation of the tropical precipitation in the National Center for Atmospheric Research Community Climate Model, version 3. *J. Geophys. Res.,* **110,** D09109, doi:10.1029/2004JD005617.